INTERNATIONAL ATOMIC ENERGY AGENCY
UNITED NATIONS EDUCATIONAL, SCIENTIFIC AND CULTURAL ORGANIZATION

INTERNATIONAL CENTRE FOR THEORETICAL PHYSICS
34100 TRIESTE (ITALY) - P.O.B. 586 - MIRAMARE - STRADA COSTIERA 11 - TELEPHONE: 2240-1
CABLE: CENTRATOM - TELEX 460392 - I

SMR/388 - 25

SPRING COLLEGE IN MATERIALS SCIENCE ON "CERAMICS AND COMPOSITE MATERIALS" (17 April - 26 May 1989)

PHASE DIAGRAMS (Lecture II)

J.A. ALONSO
Departamento de Fisica Teorica
Universidad de Valladolid
Facultad de Ciencias
47011 Valladolid
Spain

PHASE DIAGRAMS*

J.A. ALONSO
DEPARTAMENTO DE FISICA TEORICA
UNIVERSIDAD DE VALLADOLID
SPAIN

* Lecture presented at the Spring College in Materials Science on Ceramics and Composite Materials (ICTP - Trieste April - May 1989).

1. INTRODUCTION[1]

The result of mixing together two (or more) metals may be quite complex. Small concentrations of a solute metal in a given solvent metal may form a "solid solution", in which the crystal structure of the solvent is maintained, although the dimensions of the unit cell may change. When the atoms of the two metals are of similar size the solute atoms may replace those of the solvent (substitutional solid solution), while if the solute atom is much smaller than the solvent atom then the solute atoms may occupy "interstitial" positions between the atoms of the solvent.

At higher solute concentrations the different types of atom may be together accomodated in crystal structures which are different from those of the components, forming stable configurations known as intermediate phases, with a given stoichiometry (for instance A_3B, or AB, etc.).

Thermodynamics controls the phases that actually appear in a given binary (or ternary, etc) system. In any system at fixed temperature T and pressure p, the Gibbs free energy G must be a minimum for stability. G can be expressed

$$G = U - TS + pV \qquad (1)$$

where U is the internal energy, S the entropy and V the volume. In alloy systems at atmospheric pressure pV can be neglected and the equilibrium condition is that the Helmholtz free energy $F = U - TS$ should be a minimum.

For a pure metal F is a function of T. For an alloy F is a function of both T and composition; for a given T it is possible to plot F for a given alloy structure against composition, obtaining a curve which has a minimum. The formation of a stable solid solution is accompanied by a decrease of the free energy of the solvent metal. Intermediate phases are characterized by a free energy which has a minimun at a given stoichiometry and that raises rapidly for compositions off-stoichiometry. Systems of two or more components will always assume a condition, in equilibrium, of lowest free energy. It then follows that the structures which are actually stable at various compositions depend upon the relative free energies of all the possible configurations of the system at the temperature considered. Equilibrium between them is reached when the total free energy is a minimum. Furthermore, since these relative free energies change with T, the equilibrium state of the system will be different, for a given composition, at different temperatures.

The phase diagram provides a way of summarising the state of the system as a function of composition and temperature.

2. DERIVATION OF SIMPLE TYPES OF PHASE DIAGRAM FROM FREE ENERGY PRINCIPLES

2.1 Complete miscibility

As an example of how to construct a phase diagram we concentrate on the case of complete miscibility in a binary alloy. Consider a system A-B in which the two metals have the same crystal structure and form a complete series of solutions with each other in both the liquid and solid states, without intermediate phases. At a temperature T, such that the system is liquid at all compositions, the free energy of the liquid and solid solution have the form shown is Fig. 1. The free energy of the liquid is below that of the solid at any composition. If T is now lowered the free energy curves come closer together. At a temperature T_2 the two curves first touch. This occurs at a point of the left-hand vertical free energy axis. At T_2 solid A and liquid A have the same free energy. T_2 is the frezing temperature of metal A. A further temperature lowering leads to the situation in Fig. 2, in which the two curves cross. At temperature T_3 alloys which composition between A and p adquire the lowest possible free energy if they are in the solid state as solid solutions of B in A. Alloys of composition between q and B have the lowest free energy if they exist as a liquid mixture of A and B. Any alloy of composition between p and q will have the lowest free energy as a mixture of solid solution of composition p and liquid mixture of composition q. So, at T_3, solid of composition p exists in equilibrium with liquid of composition q. The composition of the solid and liquid in mutual equilibrium are defined by the points of contact of a common tangent to the two free energy curves, and conditions for equilibrium may be written:

$$(\partial F_m/\partial c)_{c_m} = (\partial F_l/\partial c)_{c_l} \qquad (2)$$

$$\partial F_m/\partial c = (F_m - F_l)/(c_m - c_l), \qquad (3)$$

where F_m and F_l are the free energies of the solid and liquid respectively, and c represents composition. c_m and c_l are the composition of solid and liquid in mutual equilibrium.

Further decreare of temperature results in the point of intersection X moving towards the right of the free energy diagram. This is accompanied by a corresponding shift, in the same direction, of the common tangent defining the compositiom of solid and liquid in mutual equilibrium. Finally, at the temperature of freezing of metal B the two curves will intersect at the right-hand vertical free energy axis. Below this temperature the F_s curve lies entirely below F_l and the system exists as a mutual solid solution of A and B.

The composition of the solid and liquid phases which are in equilibrium at the various temperatures may now be plotted on a diagram having a temperature axis as ordinate and a composition axis as abscissa. This forms the phase or equilibrium diagram. the form of the phase diagram for the system discussed is given in Fig. 3. The curve LNO is known as the liquidus curve. Alloys at a temperature and composition above the liquidus curve consist of a single liquid phase. Below the solidus curve (the curve LNO) the alloys exist in the solid solution phase. Alloys falling within the area LMON consist on a mixture of solid and liquid phases. For instance, at temperature T_3 the compositiom of solid and liquid are p and q. At composition r and temperature T_3 the alloy consists of solid and liquid phases in the ratio rq/pr, since this ratio minimizes the free energy. This relation is known as the Lever Rule.

The precise form of equilibrium diagram for an alloy system of the type described above depends upon the relative shapes of the two free energy cruves. If the relative shapes are like in Fig. 4, then at some lower temperature the two curves will touch at an intermediate composition, giving rise to an equilibrium diagram in which the liquidus and solidus exhibit a maximum as shown in Fig. 5.

2.2 Limited mutual solid solubility

The forms of phase diagram to be expected when the atomic diameters of A and B are comparable, the valencies equal or similar, but the crystal structures different are now considered. The components may be expected to dissolve completely in each other in the liquid state, an each to dissolve appreciable quantities of the other in the solid state. These systems lead to phase diagrams of the form shown in Fig. 6.

In Fig. 6(a) at temperature T_E and compositions between p and t,

liquid of composition e is in equilibrium with solid α of composition p and solid β of composition t. The composition e is known an the eutectic composition. Liquid of this composition solidifies at the eutectic temperature T_E to form a mixture of the two solid phases of compositions p and t respectively, in the proportions et/pe. Under equilibrium conditions the temperature remains constant until solidification is complete.

In the phase diagram of fig.6(b), at the temperature T_P and no other, three phases are again in equilibrium: liquid of composition p_1, α of composition p_2 and β of composition t. The composition p_1 is known as the peritectic composition. The significance of this diagram is that, at T_P, liquid of composition p_1 reacts with α of composition p_2 to form β of composition t.

The course of solidification is easily followed from Figs 6(a) and 6(b). The maintenance of equilibrium demands that diffusion in the solid state be sufficiently rapid to ensure that the composition of the solid is at all times uniform throughout and is that corresponding to the equilibrium diagram at any given moment during the course of solidification. In practical cases diffusion is usually too slow for this to occur.

2.3 Systems which include intermediate phases

In many systems, one or more distinct phases, with crystal structures different from those of either of the terminal solid solutions, may be formed within certain composition ranges. These are known as Intermediate Phases. A typical phase diagram is given in Fig. 7.

2.4 Systems involving solid state reactions

In all the examples so far considered, it has been assumed that the solid phases, once formed, are stable from the temperature of their formation to the lowest temperature at which observations are possible. This is not necessarly true. By analogy with the eutectic, the point F in Fig. 8(a) is called a Eutectoid Point. The process by which the phase AB of composition f splits up at the fixed temperature T_F into α of composition g and β of composition h is known as a eutectoid transformation. Similarly, phases may be formed in the solid state by a process analogous to a peritectic reaction. Fig. 8(b) shows an example in which, at the

temperature T_1, α of composition j and β of composition l react together to form a new phase, α, of composition K. Such eutectoid and peritectoid reactions in the solid state are frequently sluggish, and may need considerable time for completion.

A further feature often encountered in binary phase diagrams is the transformation of a solid phase into another, crystallographically distinct, phase with similar composition, as the temperature is decreared or increased. The simplest case is the allotropy of a pure metal. In this case the transformation takes place at constant T and latent heat of transformation is involved. When such a polymorphic change occurs in component A of a binary system, the transformation temperature may be raised or lowered by the presence of the other component (see, for instance, Fig. 9) Similar transformations may take place in intermediate phases (Fig. 10).

3. RELATION BETWEEN SURFACE SEGREGATION AND PHASE DIAGRAMS IN BINARY SOLID ALLOYS[2]

The composition of an alloy surface is usually not identical with its bulk composition. Rigorously, Γ, the excess surface concentration of one component over its bulk concentration c in related to the composition dependence of the surface tension $d\gamma/dc$ by

$$\Gamma = - \frac{c}{RT} \frac{d\gamma}{dc} . \qquad (4)$$

This implies that one component of the alloy should segregate to its surface if the surface tension decreases with increasing concentration c of that component. The problem is that little is known about $d\gamma/dc$.

Burton and Machlin[3] proposed a simple rule to predict surface segregation in solid alloys. This rule is based on consideration of the melting curve of the alloy.

The suggestion of these authors is to relate surface segregation to the equilibrium distribution of a solute in an alloy to its liquid. This is reasonable since many of the aspects that distinguish a liquid from a solid (lower symmetry, often lower coordination number and no elastic strain)

also distinguish a solid from a surface. They therefore aserted that segregation should occur in the solid/surface equilibrium if and only if distribution occurs in the solid/liquid equilibrium in such a way that the liquid is richer in solute than the solid phase. The two type of solid/liquid equilibrium curves that are the basis for predicting distribution of solute from the solid to the liquid are shown in Fig. 11, Fig. 11(b) represents a segregation system. If a solid containing 5% solute were heated to its solidus temperature (dashed curve) then liquid would begin to form containing a solute concentration of ~ 10%; thus solute would distribute from the solid to the liquid. For fig. 11(a), if a 5% alloy were heated to its solidus temperature then the liquid formed would contain only ~ 2% solute; thus solute distribution from the solid to the liquid would not occur.

Burton and Machlin therefore proposed that any dilute binary alloy with a melting curve of the type in fig. 11(a) should not exhibit segregation. Those with melting curves of the form of fig. 11(b) can show surface segregation. If the separation between the solidus and liquidus curves is large then copious surface segregation should occur. The agreement between the model predictions and experiment is rather good.

4. PHASE TRANSFORMATIONS [4]

The driving force in phase transformations in the solid state (at constant p and T) is the net decrease of the Gibbs free energy. However, the mode of transformation is very dependent of the effects of small fluctuations from the initial condition. Most phase transformations start from identifiable centers, a process known as nucleation, and the transformed regions then grow into their surroundings. Regions of discontinuity (macroscopic surfaces) are then introduced during transformation. Many solid state transformations which begin from nuclei are dependent on thermally activated atom movements for the subsequent growth of these nuclei. In typical reactions of this kind, a new phase grows at the expense of an old phase by the relatively slow migration of the interphase boundary, the velocity of which varies markedly with temperature.

Classical theory of nucleation

Consider the formation of a small region of a new phase (β) in the interior of the parent phase (α), and assume that the two phases have the same composition. When both phases are solid, the formation of a β region may leave the assembly in a self-stressed condition. The resulting stress energy can be written $N\Delta g_s$, where N is the number of atoms in the nucleus, and Δg_s the stress energy per atom. This energy will be much larger for a nucleus that is coherent with the matrix than for an incoherent nucleus. The surface area of the nucleus can now be written $\eta N^{2/3}$, where η is a geometrical factor depending on the shape. If the free energies per atom in the bulk phases are g^α and g^β respectively, the net free energy change on forming the nucleus is

$$\Delta G = N(g^\beta - g^\alpha) + \eta N^{2/3}\gamma + N\,\Delta g_s \qquad (5)$$

where γ is the surface energy per unit area. This equation shows that transformation cannot begin until the effective driving force $\Delta g' = g^\alpha - g^\beta - \Delta g_s$ becomes positive. In this case the variation of ΔG with N for any nucleation path will have the form shown in Fig. 12, there being a nucleation barrier, that is, a maximun free energy increase ΔG_c at a critical nucleus of size N_c. The most favorable nucleation path will choose nuclei of size, shape and type such as to minimize the nucleation barrier.

Coherent nuclei will usually have small surface energy terms but large strain energies. Incoherent nuclei will have much larger surface (misfit) energies, but smaller strain energies. The surface energy term will be dominant for sufficiently small nuclei, but will decrease in importance as the nuclei grow. For all the β regions there is thus a tendency for the smallest nuclei to be coherent with the matrix, and for the larger nuclei to become incoherent. It follows from eq(5) that N_c and ΔG_c are given by

$$N_c = (2\eta\gamma/3\Delta g')^3 \qquad (6)$$

$$\Delta G_c = (1/3)\eta N_c^{2/3} = 4\eta^3\gamma^3/27(\Delta g')^2. \qquad (7)$$

Nuclei of size N_c are in an unstable equilibrium with the α phase, those of size $N<N_c$ have a tendency to grow into macroscopic β regions. Both N_c and ΔG_c decrease rapidly as the driving force $\Delta g'$ increases.

The classical theory assumes that nuclei grow by the addition of individual atoms, so that a stable nucleus is formed only as a result of a favorable series of fluctuations. In the early stages of transformation, a quasi-steady distribution of nuclei of various sizes may be established,

the concentration of nuclei of any one size and shape varying very slowly in time. We can define a steady-state nucleation rate I as the number of stable nuclei produced in unit time in unit volume of untransformed α. Theories lead to the result

$$I\alpha \exp(-\Delta G_c/KT). \tag{8}$$

The rate at which individual nuclei grow will also be dependent on the frequency with which atoms adjacent to the nucleus can join it, and this may be written $v\exp(-\Delta g_m/KT)$, where v is a characteristic vibrational frequency and Δg_m is an activation energy for atomic migration. If the β and α phases have the same composition, Δg_m may be identified with the activation energy for the movement of an atom across the interface region. When the nucleus has a different composition Δg_m should be the free energy of activation for the diffusion of the slower moving atom.

An approximate expression for the nucleation rate is now

$$I = N_v\, v \exp(\Delta g_m/KT) \exp(-\Delta G_c/KT) \tag{9}$$

where N_v is the number of atoms per unit volume in the α phase. I varies very rapidly with temperature. For solids I is well approximated by

$$I \approx 10^{30} \exp(-\Delta G_c/KT). \tag{10}$$

A nucleation rate of one nucleus per cm^3 sec, which is an estimate of the minimum rate which could be observed experimentally, thus corresponds to $\Delta G_c \sim 70$ KT. A nucleation rate a million times larger is obtained if the driving force is increased so that $\Delta G_c \sim 55$ KT. It is reasonable to take $(g^\alpha - g^\beta)\ \alpha \Delta T/T^{\alpha\beta}$, where ΔT represents the supercooling from the eqilibrium transformation temperature $T^{\alpha\beta}$. It then follows from eq. (7) that the million fold increase in nucleation rate is achieved by increasing the supercooling by a factor $(70/55)^{1/2}$. Then, if the nucleation rate is just perceptible at a supercooling of, say, 50 °C, it will be very rapid at a supercooling of 55°C. The rapid variation of nucleation rate with driving force is characteristic of all nucleation processes.

For a transformation on cooling, I increases rapidly from zero at $T^{\alpha\beta}$ but eventually decreases again. The decrease is due to the factor $\exp(-\Delta g_m/TK)$. since Δg_m is nearly independent of T. In contrast, the rate of a transformation on heating increases continuously as T is increased above the transformation temperature, since both factors now work in the same sense.

Finally we want to point out that the above theory can be extended

without difficulty to the case of Solidification. In this case a solid forms from its melt. It is evident that the strain energy (the third term on the r.h.s. of eq. (5)) in negligible in this case since the matrix is liquid. Also, Δg_m must be identified with the free energy of activation for diffusion in the melt ($\Delta g_m \sim KT$).

Heterogeneous nucleations

Nucleation from a fluid phase is frequently catalysed by solid impurities which reduce the energy needed to create a nucleus of critical size. This is called heterogeneous nucleation and it is readily included in the formalism of the classical theory by assuming that the free energy of part of an existing surface which is destroyed helps to provide the energy of the nucleus. A similar formal extension of the classical theory may be made for heterogeneous nucleation in the solid state, where nuclei form preferentially on grain boundaries or dislocations. The surface energy of a grain boundary or a stacking fault, or the strain energy of a dislocation line, may then be assumed to reduce the formation energy of a nucleus.

5. DESCRIPTION OF COMPOUND STRUCTURE

5.1 Hume-Rothery electron compounds

There is a well known correlation, for transition metals, between the crystal structure and the number Z of valence (d+s) electrons. This is shown in Table 1. In a pioneering work, Hume-Rothery[5] correlated the crystal structure with the average number of valence electrons per atom, $\bar{Z}$, for alloys of noble metals with sp-elements. Taking Z=1 for the noble metals, then the disordered fcc α-phase, which is characteristic of the noble metal-rich alloys, is observed to exist up to $\bar{Z} \approx 1.38$, the bcc β-phase to be stable around 1.48, the γ phase around 1.62 and the hcp ϵ-phase around 1.75. Mott and Jones [6] proposed an explanation of this effect within Nearly-Free-Electron theory. They pointed ont that the fcc and bcc electron-per-atom ratios correlate with the number of electrons at which a free-electron Fermi sphere first makes contact with the innermost face of the fcc and bcc first Brillowin zone, $\bar{Z} = 1.36$ and 1.48 respectively. Then,

as soon as the concentration, and consequently $\bar{Z}$, are increased, the crystal structure changes in order to accomodate all of the valence electrons within the first Brillonin zone, minimizing the band energy. In summary, Mott and Jones assigned a special stability associated with having all the electrons in the first zone.

5.2 Empirical description of compound structure

Apart from the electron per atom ratio, other factors have been considered important in determining structural stability. Examples are atomic size, core size, electronegativity, and atomic energy level of the constituents. Beginning with the work of Mooser and Pearson [7] many workers have constructed two-dimensional structural maps with the objective of separating the different crystal structures of binary compounds of the map in an empirical way. In the work of Mooser and Pearson the coordinates were: the difference of electronegativity, ΔX, and the average principal quantum number (of the outermost occupied shell of the atom). More recently, other coordinates have been tried. For instance, in Fig. 13 we show a map for the so-called binary octet compounds. The coordinates used are R_σ^{OP} and R_π^{OP}. These are constructed from s and p pseudopotential radii, calculated by Zunger [8] using Density Functional theory

$$R_\sigma^{OP} = |(r_p^O + r_s^O) - (r_p^M + r_s^M)| \qquad (11a)$$

$$R_\pi^{OP} = |r_p^O - r_s^O| + |r_p^M - r_s^M|. \qquad (11b)$$

r_s and r_p are effective core radii "seen" by outer s and p electrons respectively.

It is evident that the map is very successful. This and similar work is of great value. First, it is still difficult for first principles calculations to predict the equilibrium structure of a compound. Besides, it is not trivial to deduce from first-principles calculations what are the main physical factors controlling the relative stability of different structures. Secondly, the maps can be used with predictive purposes. Recent work by Pettifor [9] is an outstanding step to connect the empirical descriptions of structure with band theory concepts.

5.3 Formation of compounds versus non-formation

We have briefly considered above the question of what crystal structure is adopted by an intermetallic compound of given stoichiometry. Related to this one is the question of which binary systems form intermetallic compounds and which systems do not. Villars[10] has found three coordinates that permit systems that form compounds to be separated from those that do not form by means of two three-dimensional diagrams. The first diagram applies to combinations of isostructural elements and the other to combinations of elements with different crystal structures. In total, 3916 binary systems were considered, The method of separation has an accuracy of 96%. The three coordinates are (i) the magnitude

$$\Delta(r_s + r_p)_{AB} = |(r_s + r_p)_A - (r_s + r_p)_B| \qquad (12)$$

of the difference between Zunger pseudopotential radii sums, (ii) the ratio T_A/T_B of the melting temperatures ($T_A > T_B$), and (iii) the magnitude $|\Delta Z|$ of the difference between the number of valence electrons. In addition, the systems that do not form compounds can be separated into four different types: (a) the solubility type; (b) the insolubility type, (c) the eutectic type; (d) the peritectic type.

As a further step Villars [11] has shown that the three-dimensional stability diagram can also be applied to distinguish between compound formation and absence of compounds in ternary systems. The database is from 7200 ternary systems, which represent a small fraction (<10%) of all the possible ternary combinations. The separation obtained is accurate to 94%. As an extension of the coordinates to the ternary case, Villars formed

$$\frac{1}{3}\,(|\Delta r_{AB}| + |\Delta r_{BC}| + |\Delta r_{AB}|), \qquad (13a)$$

$$\frac{1}{3}\,(|\Delta Z_{AB}| + |\Delta Z_{BC}| + |\Delta Z_{BC}|), \qquad (13b)$$

$$\frac{1}{3}\,\left(\frac{T_A}{T_B} + \frac{T_A}{T_C} + \frac{T_B}{T_C}\right). \qquad (13c)$$

It was found that the space of non-compound formation is very simple. This is plotted in Fig. 14. Roughly speaking, no compound formation occurs along the three axes of the stability diagram.

6. FACTORS AFFECTING THE FORMATION OF SOLID SOLUTIONS[2]

The extent of solid solubility results normally from a competition between terminal and intermediate phases. Hume-Rothery extensively studied the factors that determine the formation of solid solutions. Even today, those factors form the basis of our present understanding of these systems.

Size factor

The size rule states that solid solutions are not expected if the atomic sizes of solute and solvent differ by more than 15%. A favorable size factor is then a necessary (but not a sufficient) condition. Since a solid solution preserves the crystal structure of the host, large elastic stress is introduced by the atomic size difference, which opposes extensive solubility. Eshelby and Friedel applied elasticity theory to the problem of introducing a sphere of volume V_A into an spherical hole of size V_B in a matrix B. The energy increase in that process is

$$\Delta H^{\infty}(A \text{ in } B) = \frac{2\mu_B}{3+4K_A\mu_B} \quad \frac{(V_A - V_B)^2}{V_B}, \qquad (14)$$

where K_A is the compressibility of the solute and μ_B the shear modulus of the host. From this expression, the Hume-Rothery rule can be justified.

Electrochemical factor

Hume-Rothery's second rule states that the electrochemical nature of the two elements must be similar if solid solutions are to be expected. If, however, their electrochemical natures are very different, formation of compounds is likeky to occur. A measure of the electrochemical nature of an element is provided by its electronegativity. A difference $\Delta X = X_A - X_B$ in electronegativity induces a transfer of electronic charge that favors chemical ordering and formation of compounds. The contribution to the binding enthalpy is proportional to $-(\Delta X)^2$. The proportionality constant involves the number of B-neighbours around an A atom; then the preference for compound formation becomes clear. Only when $|\Delta X|$ is small is the entropy of random mixing able to stabilize a solid solution.

Darken and Gurry (DG) used simultaneaously the size and electrochemical factors [12]. Using atomic radius and electronegativity as

coordinates of a two-dimensional map for binary alloys based on a given host metal, they observed that highly soluble elements cluster around the host coordinates in the map and can be separated from the insoluble elements by drawing an ellipse centered on the host (see Fig. 15 for Ag alloys). It is clear why soluble elements cluster around the host coordinates: a large size difference opposes the formation of solid solutions, and a large ΔX favours the formation of ordered compounds. The DG coordinates have also been applied to metastable solubility obtained by ion implantation. Substitutional implants can then be separated from interstitial implants.

Relative valence effect

Hume-Rothery's third rule states that a higher-valent metal is more soluble in a lower-valent metal than viceversa. Recent work by Goodman and coworkers has clarified the status of this rule[13] in the case of transition metal alloys. Fig 16 serves to illustrate the discovery of these authors. The chart can be separated in two regions by a diagonal boundary (the cross-hatched region). Only in one of the regions is the relative valence rule obeyed. In contrast in the other region the lower-valent metal is more soluble in the higher valent metal. The trend in this figure can be rationalized in terms of d-band filling. If the boundary region where the diagonal involving the dotted rather than the cross-hatched squares, then the observed rule could be summarized by stating that, whichever transition metal has a more-nearly half-filled d-band then that metal prefers being the solute rather than the solvent. The actual boundary is one set of squares to the left, so the trend obeys a "left-shifted" half-filled d-band rule.

Miedema coordinates

In 1979 Chelikowsky presented solubility plots in which the two coordinates are borrowed from Miedema's theory (see section 7 below): electronegativity (X) and electron density at the boundary of atomic cells in the bulk metal (n_{ws}). These coordinates lead to a separation between soluble and insoluble elements (in a given host) more accurate than the DG coordinates. Noticing that X is common to the two sets of coordinates mentioned above, Alonso and Simozar[14] considered X, V and n_{ws}, and combined X

and n_{ws} in a single coordinate to again produce a two-dimensional map. To combine X and n_{ws} they used Miedema's expression for the heat of formation of a liquid alloy $\Delta H_1(A/B)$. The corresponding plots of $\Delta H_1(A/B)$ versus (V_A-V_B), with B fixed, lead to an improved separation between soluble and insoluble elements (see an example in Fig. 17).

7. THE MODEL OF MIEDEMA AND RELATION TO PHASE DIAGRAMS

With the assumption that the electronic rearrangements at the contact beween atomic ells of A and B atoms in an alloy are similar in essence to those occurring between two macroscopic pieces of metals A and B in contact, Miedema[15] arrived at the following semiempirical relation for the heat of formation of liquid alloys of two transition metals or two non-transition metals

$$\Delta H \alpha \{-P(\Delta X)^2 + Q(\Delta n_{ws}^{1/3})^2\} \qquad (15)$$

where P and Q are universal constants. The first term favours the formation of the alloy and is due to charge transfer effects. The second term opposes alloy formation and comes from the energy increase due to healing the original discontinuity in the electron density at the boundary between A and B atomic cells in contact. The term in brackets in eq. (15) must be multiplied by an appropriate function of the concentrations and atomic volumes, which takes into account the total area of contact between A and B atomic cells. In consequence this function depends on the degree of chemical order in the alloy. It is different for ordered compounds or for random alloys.

A consequence of the simple structure of eq. (15) is that the sign of the enthalpy of formation is simply determined by the ratio

$$W = \frac{|\Delta X|}{|\Delta n_{ws}^{1/3}|} \quad . \qquad (16)$$

For W > P/Q the enthalpy of alloy formation is negative, while in the opposite case the enthalpy of formation is positive. As an example of application Fig. 18 shows that eqn (15) predicts very accurately the sign

of the heat of formation for solid compounds of two transition metals. Each symbol corresponds to one binary system. • means that one or more compounds exist in the system, indicating that ΔH_{exp} (formation)<0. + indicates that there are no compounds or that both solubilities are smaller than 10 at %, indicating that ΔH_{exp} (formation)>>0. A good separation between the + and • symbols is obtained by drawing a straight line. The slope of the straight line gives the value for the ratio Q/P. Values of the parameters n_{ws}, X and constants P, Q, as well as more details on the model are given, for instance in ref. 15.

To extend the theory to alloys of one transition metal and one non-transition metal one additional term must be included in (15) accounting for the hybridization between the d-electrons of the transition metal and the p-electrons of the non-transition metal.

As it stands, eq. (15) is valid in cases like liquid alloys or solid ordered compounds. Substitutional solid solutions, in which atomic size mismatch effects play a role, as we have seen above, are beyond the scope of eq. (15). Specifically, one must then add a term accounting for atomic size mismatch effects (the term given by eq. (14)), and an structural term accounting, in the case of transition metal alloys, for the correlation observed in Table 1 between band filling and crystal structure. Details can be consulted in ref. 2.

CAPTIONS OF FIGURES

Fig. 1. Free energy curves for simple system with complete solid and liquid solubility at temperature T_1.

Fig. 2. Free energy curves for simple system with complete liquid and solid solubility, showing equilibrium between liquid and solid at temperature T_3.

Fig. 3. Equilibrium phase diagram corresponding to free energy curves in figs. 1 and 2.

Fig. 4. Different relative disposition of free energy curves for simple system with complete liquid and solid solubility at temperature T_1.

Fig. 5. Equilibrium diagram corresponding to free energy curves of fig. 4.

Fig. 6. (a) Phase diagram of an eutectic system
(b) Phase diagram of a peritectic system

Fig. 7. Phase diagram of a system with an intermediate phase.

Fig. 8. Equilibrium phase diagrams illustrating: (a) eutectoid decomposition of intermediate phase AB, and (b) peritectoid formation of intermediate phase γ.

Fig. 9. Phase diagrams illustrating the effect of allotropy of the solvent metal.

Fig. 10. Phase diagrams illustrating transformation in an intermediate phase.

Fig. 11. Typical phase diagrams for dilute alloys. From melting curves such as in (b), Burton and Machlin predict segregation of the solute to the surface of the alloy.

Fig. 12. Variation of free energy with nucleus size.

Fig. 13. A structural separation plot for 112 binary octet compounds obtained by Zunger with the density-functional orbital radii (see text).

Fig. 14. Three-dimensional stability diagram formed by Villars, showing schematically the region fo space in which compound formation occurs and that in which it does not.

Fig. 15. Darken-Gurry plot for various solutes disolved in Ag. The ellipse approximately separates soluble an insoluble impurities.

Fig 16. Experimental relative solubilities in transition-metal alloys. The dotted region indicates systems where the d-bands of the constituents are equally far from half-filled.

Fig. 17. Solubility plot for Co alloys using thermochemical coordinates.

Fig. 18. Demostration of the validity of eqn (15) for binary solid alloys of two transition metals. The meaning of the symbols is the following one: •, in the binary system one or more compounds exist, which are stable at low temperatures, indicating $\Delta H_{\bullet \times \bullet}$ (formation) < 0. + if there are no compounds in the binary system or if both terminal solubilities are smaller than 10 at %, indicating $\Delta H_{\bullet \times \bullet}$ (formation) > 0

REFERENCES

1. G. V. Raynor, Physical Metallurgy, Ed. R. W. Cahn, North Holland (1965) p. 291.
2. J. A. Alonso and N. H. March, Electrons in metals and alloys, Academic. London (1989).
3 J. J. Burton and E. S. Machlin, Phys. Rev. Lett. 37, 1433 (1976).
4. J. W. Christian, in ref. 1 p. 443.
5. W. Hume-Rothery, The Metallic State. Oxford Univ. Press (1931).
6. N. F. Mott and H. Jones, Theory of the Properties of Metals and Alloys Clarendon, Oxford (1936).
7. E. Mooser and W. B. Pearson, Acta Crystall. 12, 1015 (1959)
8. A. Zunger, Phys. Rev. B 22, 5839 (1980)
9. D. G. Pettifor and R. Podloucky, J. Phys. C. 19, 315 (1986)
10. P. Villars. J. Less-Common Metals 109, 93 (1985); 110, 11 (1985).
11. P. Villars. J. Less-Common Metals 119, 175 (1986).
12. L. S. Darken and R. W. Gurry, Physical Chemistry of Metals. Mc Graw Hill, New York (1963).
13. R. E. Watson, L. H. Bennett and D. A. Goodman, Acta Metall. 31, 1285 (1983).
14. J. A. Alonso and S. Simozar, Phys. Rev. B 22, 5583 (1980)
15. F. R. de Boer, R. Boom, W. C. M. Mattens, A. R. Miedema and A. K. Niessen, Cohesion in metals. Transition Metal alloys. North Holland. Amsterdam (1988).

TABLE 1

The structure of the Transition Metals

n	3	4	5	6	7	8	9	10	11
Period									
3d	Sc	Ti	V	Cr	(Mn)	(Fe)	(Co)	Ni	Cu
4d	Y	Zr	Nb	Mo	Tc	Ru	Rh	Pd	Ag
5d	(La)	Hf	Ta	W	Re	Os	Ir	Pt	Au
Structure	hcp	hcp	bcc	bcc	hcp	hcp	fcc	fcc	fcc

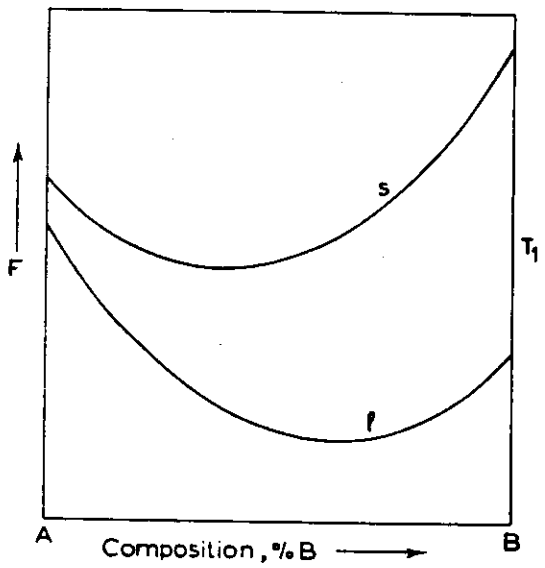

Fig. 1

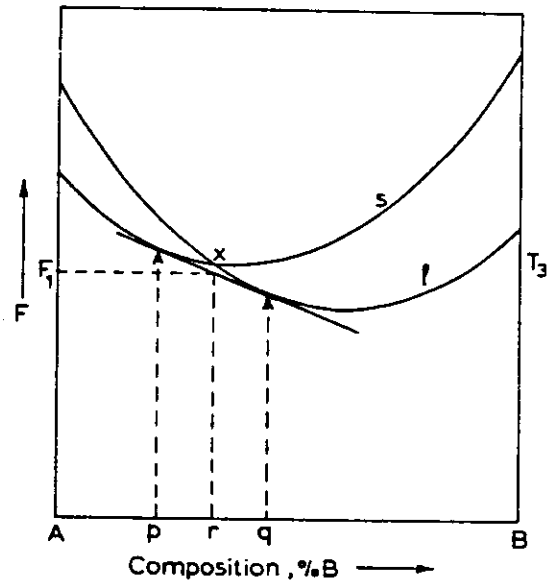

Fig. 2

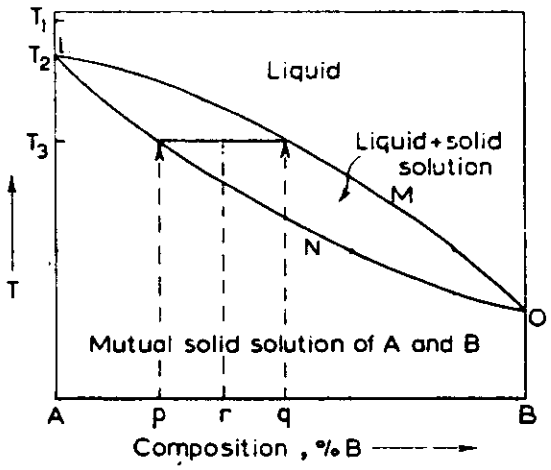

Fig. 3

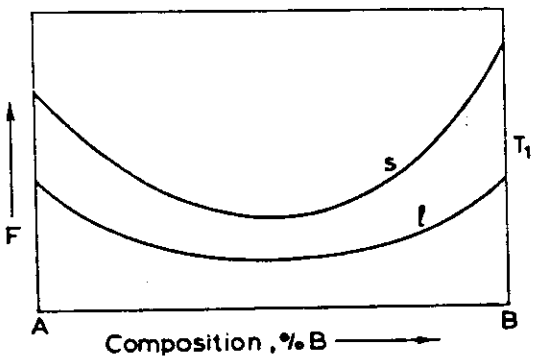

Fig. 4

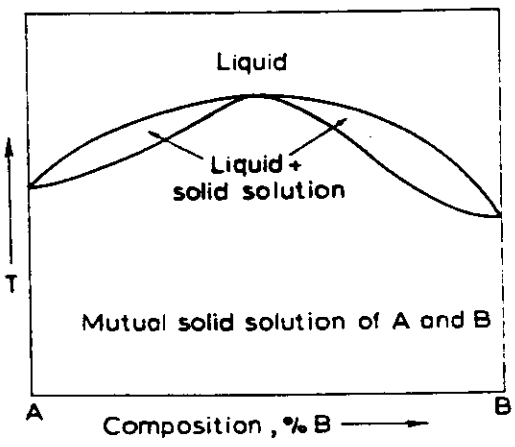

Fig. 5

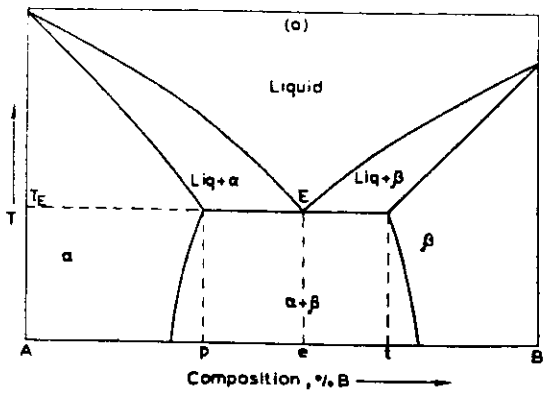
(a)
Liquid
Liq+α
Liq+β
E
T_E
T
α
β
α+β
A
p
e
t
B
Composition , %B

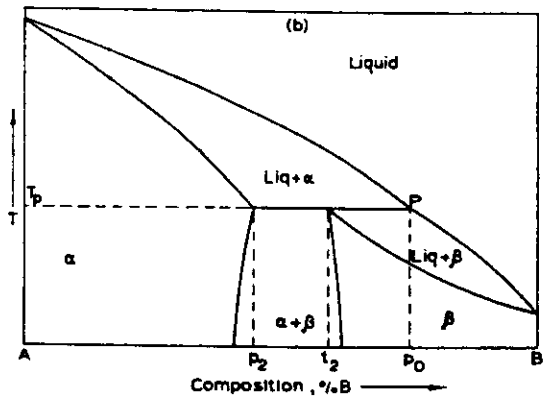
(b)
Liquid
Liq+α
T_P
T
P
α
Liq+β
α+β
β
A
P_2
t_2
P_0
B
Composition , %B

Fig 6

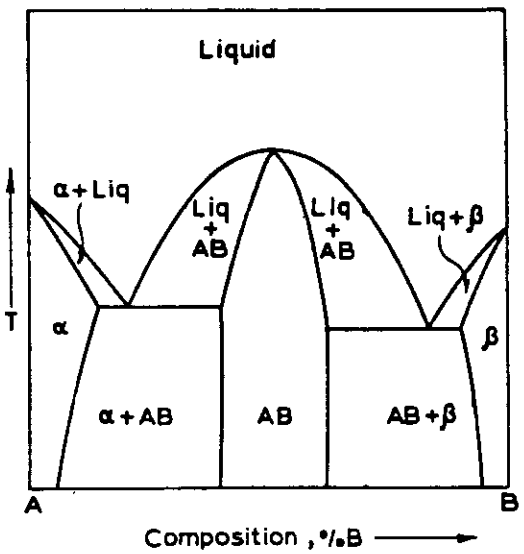
Liquid
α+Liq
Liq
+
AB
Liq
+
AB
Liq+β
T
α
β
α+AB
AB
AB+β
A
B
Composition , %B

Fig 7

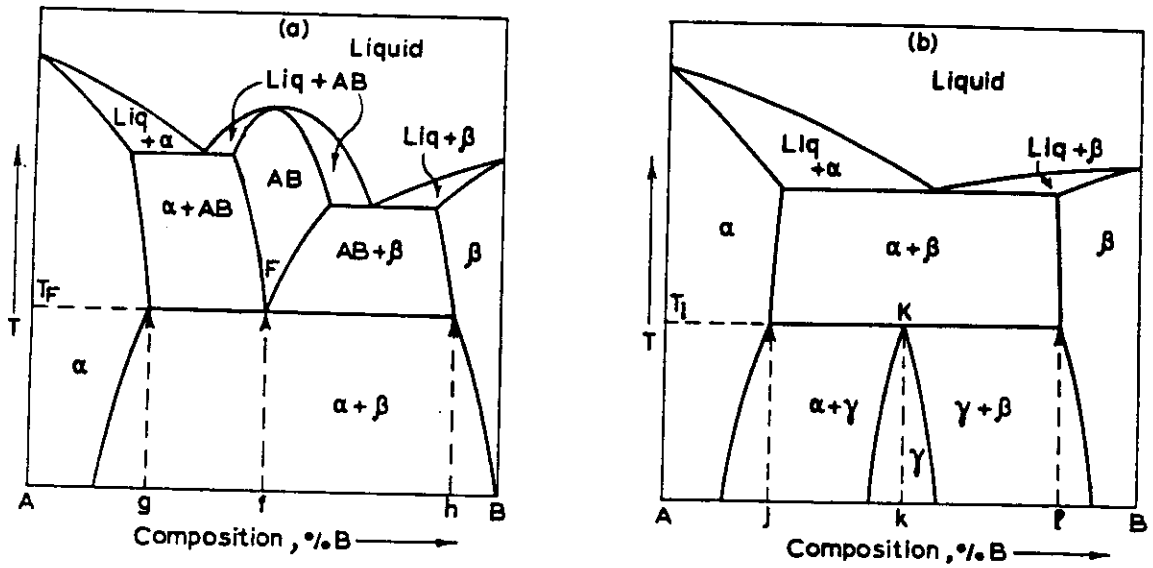
(a)
Liquid
Liq + AB
Liq +α
Liq +β
α+AB
AB
AB+β
β
F
T_F
T
α
α+β
A
g
f
h
B
Composition , %B
(b)
Liquid
Liq +α
Liq +β
α
α+β
β
T_i
K
T
α+γ
γ+β
γ
A
j
k
l
B
Composition , %B

Fig. 8

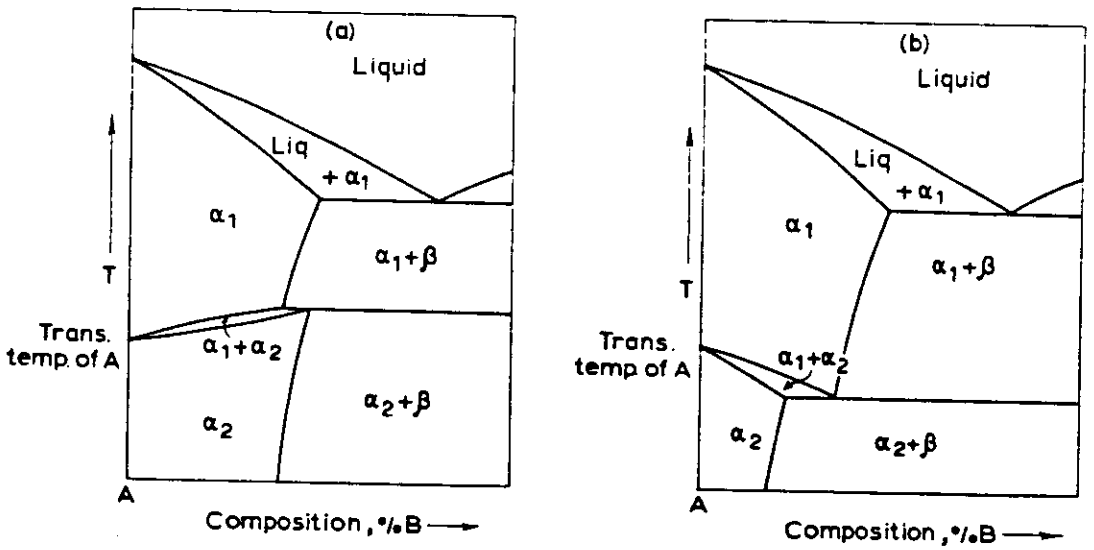
(a)
Liquid
Liq +α1
α1
α1+β
T
Trans. temp of A
α1+α2
α2
α2+β
A
Composition , %B
(b)
Liquid
Liq +α1
α1
α1+β
T
Trans. temp of A
α1+α2
α2
α2+β
A
Composition , %B

Fig 9

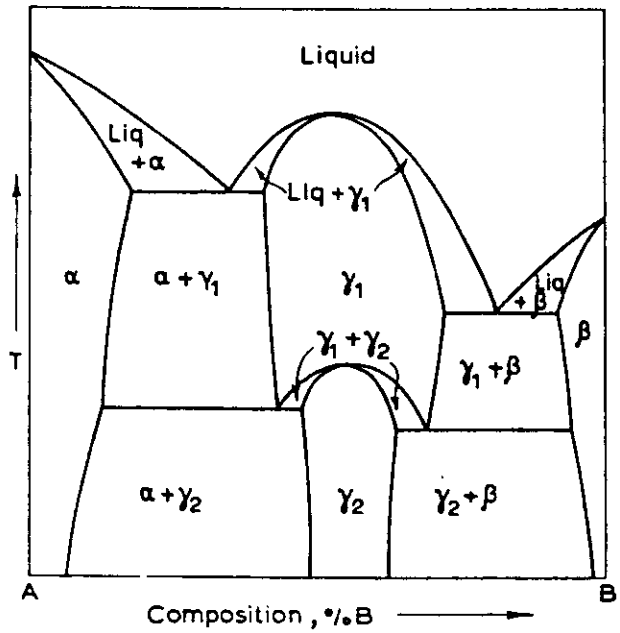

Fig 10

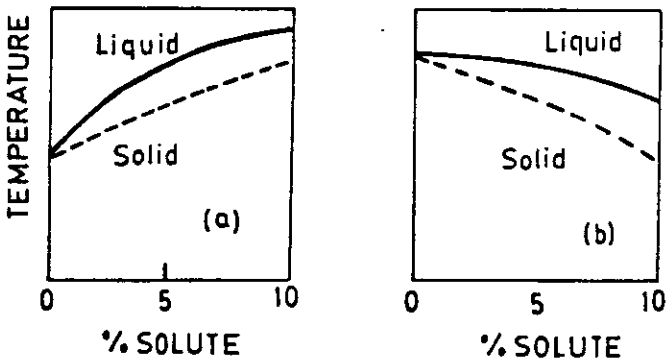

Fig 11

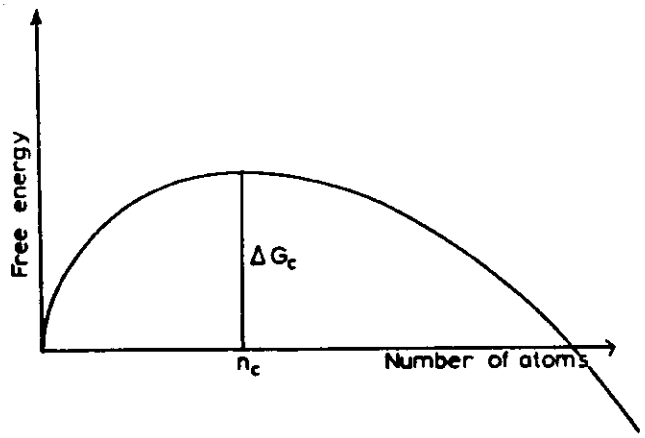

Fig 12

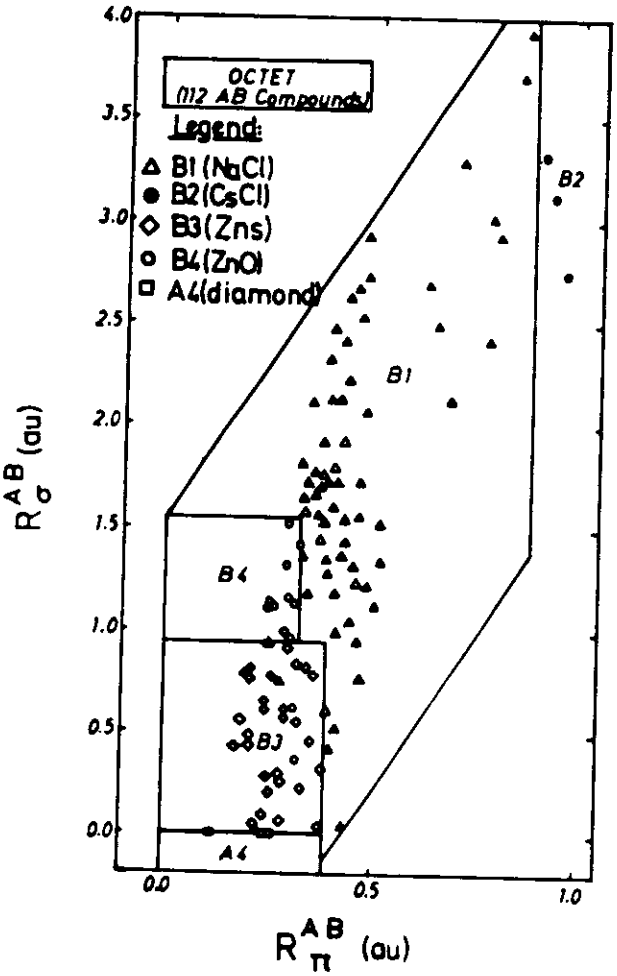

Fig 13

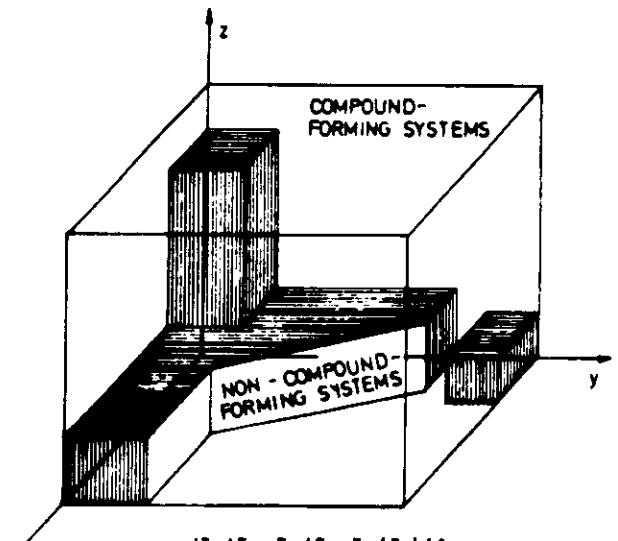

$x = (|r_A/r_B + r_A/r_C + r_B/r_C|)/3$

$y = (|\Delta r_{AB}^z| + |\Delta r_{AC}^z| + |\Delta r_{BC}^z|)/3$

$z = (|\Delta VE_{AB}| + |\Delta VE_{AC}| + |\Delta VE_{BC}|)/3$

Fig 14

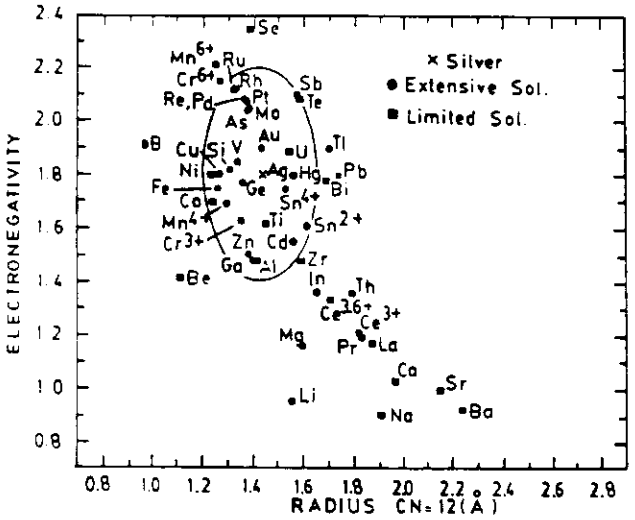
ELECTRONEGATIVITY
RADIUS CN=12(A)
× Silver
● Extensive Sol.
■ Limited Sol.
Se
Mn6+
Ru
Cr6+
Rh
Sb
Re,Pd
Pt
Te
Mo
As
Au
B
Cu
Si
V
U
Tl
Ni
Ag
Hg
Pb
Fe
Ge
Bi
Co
Sn4+
Mn4+
Ti
Sn2+
Cr3+
Zn
Cd
Ga
Al
Zr
Be
In
Th
Ce3+
Ce
Mg
Pr
La
Ca
Sr
Li
Na
Ba

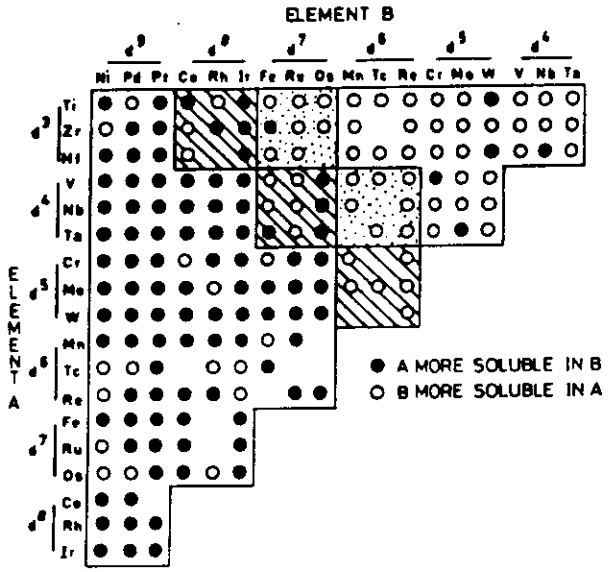
ELEMENT B
ELEMENT A
Ni Pd Pt Co Rh Ir Fe Ru Os Mn Tc Re Cr Mo W V Nb Ta
Ti Zr Hf
V Nb Ta
Cr Mo W
Mn Tc Re
Fe Ru Os
Co Rh Ir
● A MORE SOLUBLE IN B
○ B MORE SOLUBLE IN A

Fig. 6

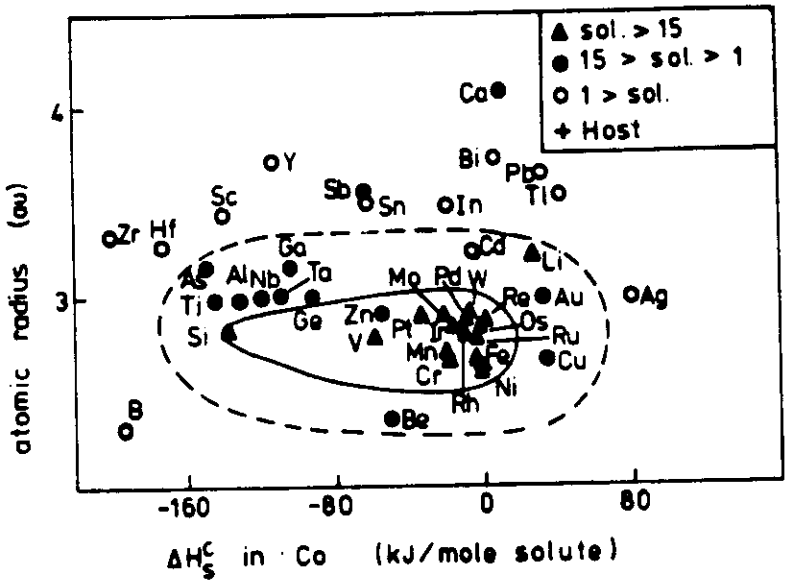
▲ sol. > 15
● 15 > sol. > 1
○ 1 > sol.
+ Host
atomic radius (au)
4
3
Co
Bi
Pb
Tl
Y
Sc
Sb
Sn
In
Zr
Hf
Ga
Cd
Li
As
Al
Nb
Ta
Mo
Pd
W
Re
Au
Ag
Ti
Ge
Zn
Os
Si
V
Pt
Ir
Ru
Mn
Fe
Cu
Cr
Ni
Rh
B
Be
-160
-80
0
80
ΔH^c_s in Co (kJ/mole solute)

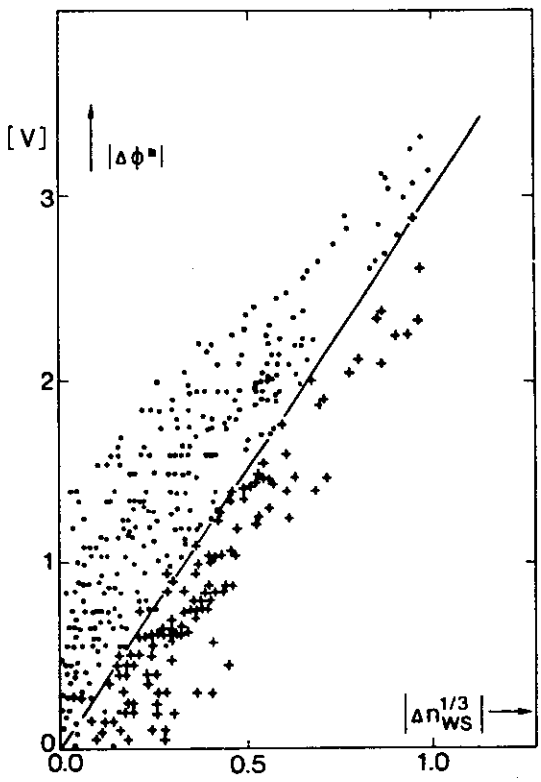
[V]
|Δφ*|
3
2
1
0
0.0
0.5
1.0
|Δn^1/3_WS|